·Article·
Advances in Polar Science
doi: 10.3724/SP.J.1085.2013.00281
December 2013 Vol. 24 No. 4: 281-295

Hydrochemistry and sediment characteristics of polar periglacial lacustrine environments on Fisher Island and Broknes Peninsula, East Antarctica

Rajesh Asthana[1*], Prakash Kumar Shrivastava[1], Hari Bahadur Srivastava[2], Mirza Javed Beg[3] & Pradeep Kumar[1]

[1] Geological Survey of India, NH 5P, NIT, Faridabad 121001, India;
[2] Department of Geology, Banaras Hindu University, Varanasi 221005, India;
[3] National Centre for Antarctic and Ocean Research, Vasco da Gama, Goa 403804, India

Received 20 May 2013; accepted 25 November 2013

Abstract Fisher Island and Broknes Peninsula in the Larsemann Hills constitute part of a polar lowland periglacial environment between marine and glacial ecosystems. The landscape is characterized by gently rolling hills and broad valleys interspersed with lakes formed in glacially scoured basins. We analyzed the physicochemical parameters and the ionic constituents of water samples from 10 lakes in each of these two locations. Our results showed considerable differences between the two regions and demonstrated the influence of lithology and processes including weathering, evaporation, and atmospheric precipitation. All major cations and anions in the lake waters showed positive correlations indicating balanced ionic concentrations. Unconsolidated sediments were sparsely distributed and scattered over glacial deposits, valley fills, and occasional moraine ridges. The type and rate of sedimentation was mainly controlled by surface run-off and aeolian influx. The sediment samples from lake beds and the catchment area on Fisher Island were immature and poorly to very poorly sorted, consisting of gravelly sand with negligible silt and finer fractions. Sediments had a polymodal grain size distribution with the two major populations lying between −2 and −1 phi and between 0 and 1.5 phi. The sediments were lithic arenite to arkosic in composition and the microtextures imprinted over quartz grains were dominated by mechanical textures resulting from several stages of glacial crushing and grinding. The presence of deep dissolution cavities, cryptocrystalline precipitation, and euhedral crystal growth signified the effect of chemical activity after the deposition of grains in the lacustrine environment.

Keywords **physicochemical parameters, lacustrine environment, ionic concentrations, microtexture, Larsemann Hills**

Citation: Asthana R, Shrivastava P K, Srivastava H B, et al. Hydrochemistry and sediment characteristics of polar periglacial lacustrine environments on Fisher Island and Broknes Peninsula, East Antarctica. Adv Polar Sci, 2013, 24:281-295, doi: 10.3724/SP.J.1085.2013.00281

1 Introduction

The Larsemann Hills area (69°20'S–69°28'S, 76°00'S–76°30'E) is an ice-free oasis on the Ingrid Christensen Coast of Princess Elizabeth Land, East Antarctica, which includes Fisher Island, Broknes Peninsula, Stornes Peninsula, and several other islands, promontories, and nunataks (Figure 1). Open sea lies to the east of Broknes Peninsula and Clemence Fjord separates it from Stinear Peninsula and Fisher Island. The deglaciated terrain constitutes a transitional zone between marine and glacial ecosystems and includes gently rolling hills, glacially polished and striated bedrock hummocks (roches moutonnees), scoured surfaces, and broad valleys interspersed with lakes of varying dimensions (Figure 2). Indian scientific studies in the Larsemann Hills started in 2003 and the present work was carried out from 2009 to 2010 during the construction of the third Indian research station, Bharati. To investigate lake water chemistry and sediment characteristics in the area we collected water samples from 20 lakes (10 each on Fisher Is-

* Corresponding author (email: rajeshasthana.antarctica@gmail.com)

land and on Broknes Peninsula) and sediment samples from lake beds and catchment areas on Fisher Island.

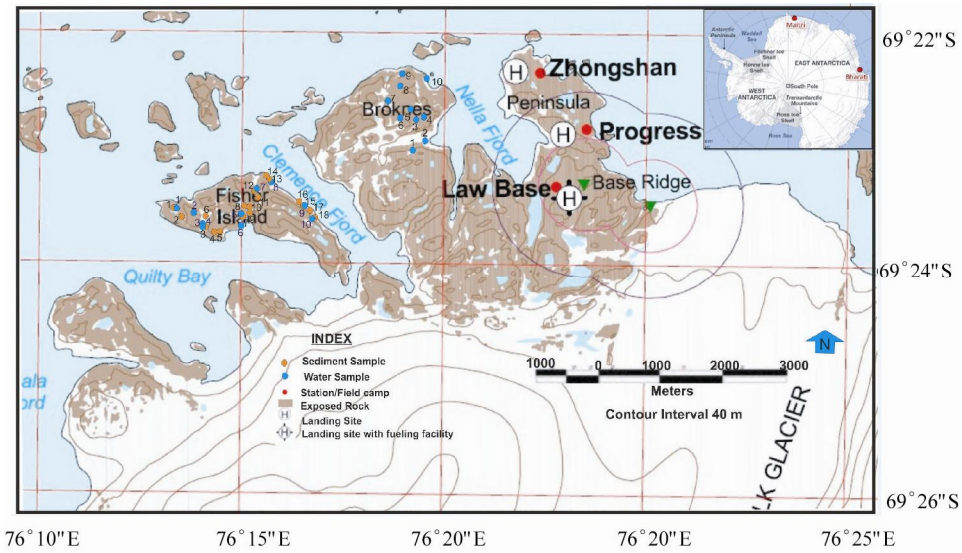

Figure 1 Location map of the area and sample sites.

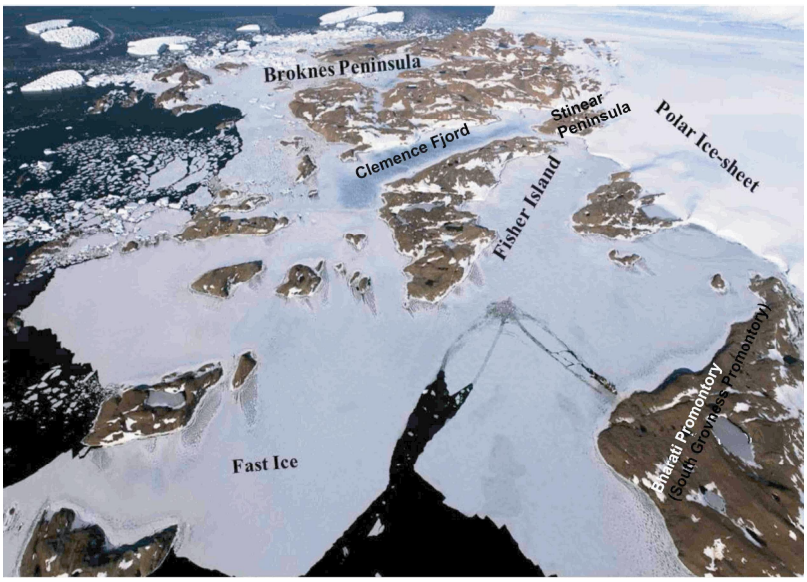

Figure 2 Physiographic elements of the study site in the Larsemann Hills.

There are more than 150 freshwater lakes in the Larsemann Hills[1] ranging from small ephemeral ponds to large water bodies. It has been suggested that many Antarctic lakes follow an evolutionary sequence as deglaciation occurs[2-3]. Lake systems are generally closed and contained in glacially scoured valleys thought to have been formed after the retreat of the continental ice cap or as a result of isostatic uplift following deglaciation[2-5]. Fisher Island is one of the large islands in the area with a maximum elevation of about 180 m above sea level. In places, valleys separate the hills and the geomorphology is controlled by lithology, geological structures, and the erosional action of ice, water, and wind. Meltwater from ice and snow controls the type and the rate of depositional processes.

Fisher Island and Broknes Peninsula in the Larsemann Hills have a polar lowland periglacial climate with relatively low precipitation, restricted periods of snow melt, and low rates of ice melt. Persistent, strong katabatic winds blow from the northeast on most days during the summer and daytime air temperatures from December to February range from 0 to 4℃. Pack ice is present adjacent to the shore throughout summer and the fjords and embayment are rarely ice-free. Weather data recorded by India Institute of Geomagnetism at an unmanned automatic weather station on Bharati Promontory (Indian Institute of Geomagnetism) between November 2009 and October 2010 showed a maximum temperature of 6.35℃ on 27 January 2010, a minimum temperature of −38.1℃ on 16 August 2010, and a maximum wind speed of 37.63 $m \cdot s^{-1}$ on 27 June 2010.

The paleoenvironment of the Larsemann Hills has

been reconstructed in a number of previous studies and the results have revealed a heterogeneous and complex history[1,3-5]. Some of the lakes have preserved the evolutionary sequence of deglaciation[2-3]. A considerable amount of work has been carried out on the glacial sediments of the Vestfold Hills and other East Antarctic coastal ice-free areas to investigate paraglacial sedimentary processes and to develop models for moraine formation[6-7]. Research on environmental parameters and freshwater lake sediments has shown that the lakes of the Larsemann Hills became seasonally ice-free after 10 500 a BP[1,8]. Previous studies have used biological and physical markers drawn from lake sediments in this region as paleoenvironmental indicators[9], and the ionic profile of lake water on the Bharati promontory and sedimentary processes in the Larsemann Hills area have also been investigated[10-11].

The Antarctic ice sheet retreated during the late Pleistocene and remained relatively stable during the Holocene epoch[12]. As a result of this temporal evolution, lakes were formed on maritime islands and peninsulas along the margins of the continent. These lakes offer a unique opportunity to study the chemical characteristics of the lacustrine ecosystem in a deglaciated terrain and to investigate the influence of the proximal ice sheet and marine ecosystems on lake hydrochemistry. During winter, the lakes become anoxic and acquire oxygen only after the frozen surface melts in summer. The mixing of fresh ice meltwater, sediment influx, and aeration take place during the summer season. The continuous cycle of freezing and melting brings about changes in the physicochemical and sedimentological properties of the water and lake bottom sediments. Summer melting of glaciers and snow banks replenishes the water lost as a result of evaporation from these lakes. Measurements of the ionic concentrations in lake waters have been widely used to investigate the influence of the lithology of the catchment, material influx into the lake systems, and other processes that influence water chemistry including weathering, evaporation, and atmospheric precipitation. Lakes on Fisher Island and Broknes Peninsula vary in depth from very shallow (a few tens of cm) to >30 m and sizes range from small ponds to a large lake with an area of 0.13 km^2. Most of the lakes on Fisher Island and Broknes Peninsula are landlocked but a few proglacial lakes on Broknes Peninsula are connected to the polar ice in the south. For the present study, sampling on Fisher Island was carried out in well-distributed representative locations but water sampling on Broknes Peninsula could be possible at a number of accessible locations only (Tables 1 and 2).

Fisher Island is typical of a polar lowland periglacial environment and is characterized by low precipitation levels

Table 1 The water sample locations from the lakes of Fisher Island

Sl. No.	Sample no.	Latitude	Longitude	Elevation from sea level/m
1	LHE/29/FI/1A & B	69°23′33.60″S	76°13′18.90″E	6.08
2	LHE/29/FI/2A & B	69°23′33.84″S	76°13′38.22″E	38.40
3	LHE/29/FI/3A & B	69°23′36.30″S	76°14′31.00″E	38.40
4	LHE/29/FI/4A & B	69°23′36.00″S	76°14′26.90″E	37.00
5	LHE/29/FI/5A & B	69°23′33.91″S	76°15′01.00″E	23.70
6	LHE/29/FI/6A & B	69°23′36.77″S	76°15′03.60″E	22.30
7	LHE/29/FI/7A & B	69°23′27.02″S	76°15′22.35″E	5.08
8	LHE/29/FI/8A & B	69°23′23.87″S	76°15′37.70″E	37.70
9	LHE/29/FI/9A & B	69°23′32.15″S	76°16″04.67″E	62.60
10	LHE/29/FI/10A & B	69°23′33.76″S	76°16′.06.56″E	58.00

Table 2 The water sample locations from the lakes of Broknes Peninsula

Sl. No.	Sample no.	Latitude	Longitude	Elevation from sea level/m
1	LHE/29/BP/1A & B	69°23′40.40″S	76°19′08.07″E	22.5
2	LHE/29/BP/2A & B	69°23′34.00″S	76°19′20.80″E	23.5
3	LHE/29/BP/3A & B	69°23′16.00″S	76°19′15.00″E	83
4	LHE/29/BP/4A & B	69°23′14.00″S	76°19′16.20″E	64
5	LHE/29/BP/5A & B	69°23′11.60″S	76°19′04.60″E	61
6	LHE/29/BP/6A & B	69°23′14.00″S	76°18′55.40″E	64
7	LHE/29/BP/7A & B	69°23′09.20″S	76°17′55.40″E	61
8	LHE/29/BP/8A & B	69°22′44.00″S	76°18′18.50″E	54
9	LHE/29/BP/9A & B	69°22′24.80″S	76°18′32.30″E	23
10	LHE/29/BP/10A & B	69°22′28.80″S	76°19′19.60″E	25

and limited snow and ice melt with only small amounts of sediment available for transportation and deposition. Debris mantles, consisting of thin deposits on hill slopes and valleys, form the only signature of glacially deposited sediments. Meltwater impounded by glacial deposits or accumulated in depressions created by glacial erosion creates snow-fed lakes of a variety of sizes, longevity, and limnological characteristics. The lakes act as sediment sinks and provide favorable locations for meltwater streams to redistribute and deposit sediments. Meltwater from ice and snow flows over the unconsolidated sediments or surficial deposits that occur as thin mantles, isolated moraine patches, or valley fills, and influences the type and rate of depositional processes. Wind also plays a significant role in reworking and depositing sediments into the low-lying lake basins.

The sediments deposited in lakes are either autochthonous or allochthonous[13] and the spatial distribution of sediments in a lake represents a complex interaction between sources in the catchment area, limnological processes occurring in the lake, and the morphology of the lake basin[14]. Sediment geochemistry and granulometric studies including grain size analysis and the examination of surface textures help in the understanding of the provenance and sedimentation process. The geochemistry of sediments from Fisher Island has shown that they are a mixture of clastic silicates and oxides (sand, silt, and clay fractions), organic material, carbonates, and water. Sediments occurring on Fisher Island are highly immature, consisting of gravelly sand with negligible silt and clay and varying proportions of pebble- to boulder-sized rock fragments. Major oxides, trace elements, and rare earth elements (REE) in the sediments have been determined.

2 Materials and methods

Helicopter-supported field work was carried out in January 2010. Water samples were collected from 10 lakes on Fisher Island and 10 lakes on Broknes Peninsula, following the standard procedure for water sample collection. Neutralized plastic bottles were rinsed twice with the lake water and duplicate samples of 1.5 L each were collected from the lakes. We assumed that chemical equilibrium had been attained and that the lake water was homogeneous during the summer period[15]. Samples were collected from easily accessible inner areas of each lake and physical parameters including conductivity, pH, and water temperature were recorded on site. One set of samples (A) was acidified using 10% (by volume) HNO_3 solution to preserve the sample and another set of samples (B) was kept for chemical analysis at the Chemical Laboratory of the Geological Survey of India (GSI). Sodium (Na), potassium (K), calcium (Ca) and magnesium (Mg) were analyzed using an atomic absorption spectrometer (Analyst-100; Perkin Elmer, Massachusetts,USA) in absorption mode using strontium salts as a buffer. Chloride (Cl^-) was analyzed using the titrimetric method with potassium chromate (K_2CrO_4) as the indicator and silver nitrate ($AgNO_3$) as the standard. A lower detection limit of 0.1 ppm for silica was achieved using a 50-mm cell in an Aquamate ThermoSpectronic Spectrophotometer. Fluoride (F^-) was measured using the zirconium-eriochrome cyanine-R method adjusted to enable accurate determination of F^- to 0.01 ppm. Carbonate (CO_3^{2-}) and bicarbonate (HCO_3^-) were determined titrimetrically using 0.01 N HCl, phenolphthalein, and methyl orange indicators. Sulphate (SO_3^{2-}) was measured to a lower limit of detection of 1 ppm using a turbidimeter according to the American Public Health Association (APHA) method. Boron (B) was analyzed using a boron test kit (Merck, Darmstadt, Germany) and nitrate (NO_3^-) was analyzed by developing color using phenol-disulfonic acid with a 50-mm cell.

Using a sediment sampler, 18 sediment samples were collected from lake beds on Fisher Island and other prominent catchment areas feeding the lake system. Sediment samples were washed with distilled water, macerated, and dried at room temperature. Mechanical sieve analysis was carried out at half phi intervals using a Retsch AS 200 sieve-shaker and ASTM sieves of #10, 14, 18, 25, 35, 45, 60, 80, 120, and 230 mesh sizes. Bigger clasts (+10 mesh) were physically measured for granulometric studies. For the study of surface textures, the standard procedure described by Krinsley and Doornkamp[13] was used for the preparation of the samples. Representative quartz grains from suitable fractions (coarse, medium, and fine) in each of the 18 samples were selected using a binocular microscope and grain morphology and surface microtextures were studied under a scanning electron microscope (SEM; Leica-S440, Germany).

3 Results

The aim of the present study of water samples from 10 lakes on Fisher Island was to determine physicochemical properties including pH, electrical conductivity (EC), total dissolved solids (TDS), and ionic concentrations (Tables 3 and 4). The pH values in the lake water ranged from 6.75 to 8.2 indicating slightly acidic to weakly alkaline conditions during the period of observation. There was a large variation in EC (26–1 179 mmho·cm^{-1}) in the water samples. The TDS ranged from 15 to 684 ppm and the ionic concentrations of the cations Na^+, K^+, Ca^{2+}, and Mg^{2+} ranged from 5.2 to 195 ppm, 0.5 to 9.6 ppm, 1.6 to 28 ppm, and 0.3 to 18 ppm, respectively. Various physicochemical parameters, ionic concentrations, and plots of the major ions within the Gibb's boomerang envelope for lake water samples from Fisher Island are shown in Figures 3 and 4[17].

The water quality parameters of the lakes on Broknes Peninsula including pH, EC, TDS, and ionic concentrations are listed in Tables 5 and 6 and presented graphically in Figure 5. The pH values ranged from 4.63 to 7.15 indicating acidic to near neutral conditions with only one lake (No. 10) showing weakly alkaline conditions. The EC (246.3–1 040 mmho·cm^{-1}) and the TDS (143–603 ppm) were also

highly variable, and the ionic concentrations of the major cations Na^+, K^+, Ca^{2+}, and Mg^{2+} ranged from 35 to 177 ppm, 1.8 to 3.8 ppm, 2.4 to 14.4 ppm, and 1.5 to 22.4 ppm, respectively. The plots of major ions within the Gibb's boomerang envelope are shown in Figure 6. In general, the lakes on Fisher Island had lower EC and TDS than the lakes on Broknes Peninsula. This difference might reflect the greater freshwater input to the Fisher Island lakes or the longer time elapsed since deglaciation on Broknes Peninsula.

Table 3 Physicochemical characteristics and ionic concentration of lake waters from Fisher Island, Larsemann Hills

Sl. No.	Sample no.	pH	EC/ (mmho·cm^{-1})	TDS	Na^+	K^+	Ca^{2+}	Mg^{2+}	Cl^-	NO_3^-	SO_4^{2-}	HCO_3^-	CO_3^-	F^-	SiO_2	B	PO_4^{3-}
1	LHE/29/FI/1B	7.21	194.1	113	31.2	1.8	5.6	2.4	57.8	0.15	9.5	15.3	0	0.07	<0.1	<0.01	0.03
2	LHE/29/FI/2B	6.75	26	15	5.2	0.5	1.6	0.3	7	0.09	3.7	6.1	0	0.07	<0.1	<0.01	0.02
3	LHE/29/FI/3B	7.49	127.4	74	15.6	1.1	4.8	6.8	35.2	0.12	8.9	21.4	0	0.10	<0.1	<0.01	0.02
4	LHE/29/FI/4B	8.20	1 179	684	195	9.6	28	18	334.1	0.16	12.2	131	0	0.01	1.86	<0.01	0.04
5	LHE/29/FI/5B	7.38	121.5	70	21.7	1.1	4	4.4	35.2	0.12	11.3	21.4	0	0.09	<0.1	<0.01	0.03
6	LHE/29/FI/6B	8.00	275.5	160	43.3	2	8	7.8	75.4	0.17	12.6	21.4	0	0.08	<0.1	<0.01	0.02
7	LHE/29/FI/7B	7.16	84	49	16	0.8	3.2	3.9	25.1	0.1	8.8	12.2	0	0.07	<0.1	<0.01	0.02
8	LHE/29/FI/8B	7.69	607.6	352	93	5	8	14.6	178.4	0.14	37	21.4	0	0.06	0.22	<0.01	0.02
9	LHE/29/FI/9B	7.81	465.6	270	81.5	1.4	6.4	5.8	128.1	0.08	26.4	24.4	0	0.06	1.64	<0.01	0.04
10	LHE/29/FI/10B	8.20	1 032	599	170	8	22	17.5	316	0.15	15.2	67.1	0	0.14	1.36	<0.01	0.05

Table 4 Correlation matrix of ionic concentration of lake waters from Fisher Island, Larsemann Hills

	Na^+	K^+	Ca^{2+}	Mg^{2+}	Cl^-	NO_3^-	SO_4^{2-}	HCO_3^-	F^-	SiO_2	PO_4^{3-}
Na^+	1										
K^+	0.96	1									
Ca^{2+}	0.96	0.96	1								
Mg^{2+}	0.92	0.94	0.88	1							
Cl^-	0.99	0.97	0.95	0.93	1						
NO_3^-	0.47	0.59	0.58	0.58	0.49	1					
SO_4^{2-}	0.36	0.27	0.11	0.46	0.37	0.03	1				
HCO_3^-	0.89	0.89	0.96	0.78	0.87	0.48	0.01	1			
F^-	-0.18	-0.16	-0.17	-0.051	-0.12	-1.4×10^{-16}	-0.14	-0.36	1		
SiO_2	0.85	0.69	0.78	0.62	0.81	0.06	0.27	0.78	-0.26	1	
PO_4^{3-}	0.76	0.64	0.72	0.53	0.75	0.16	0.13	0.64	0.14	0.84	1

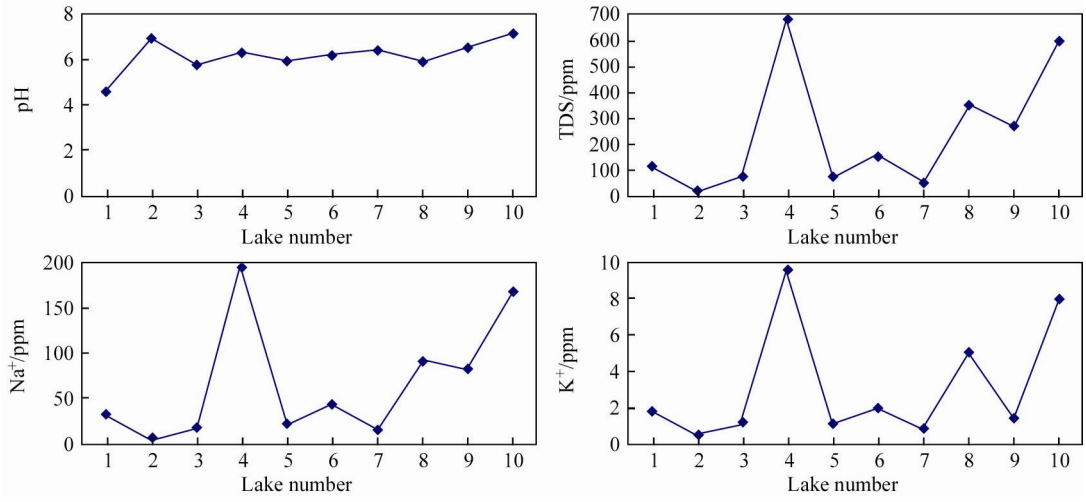

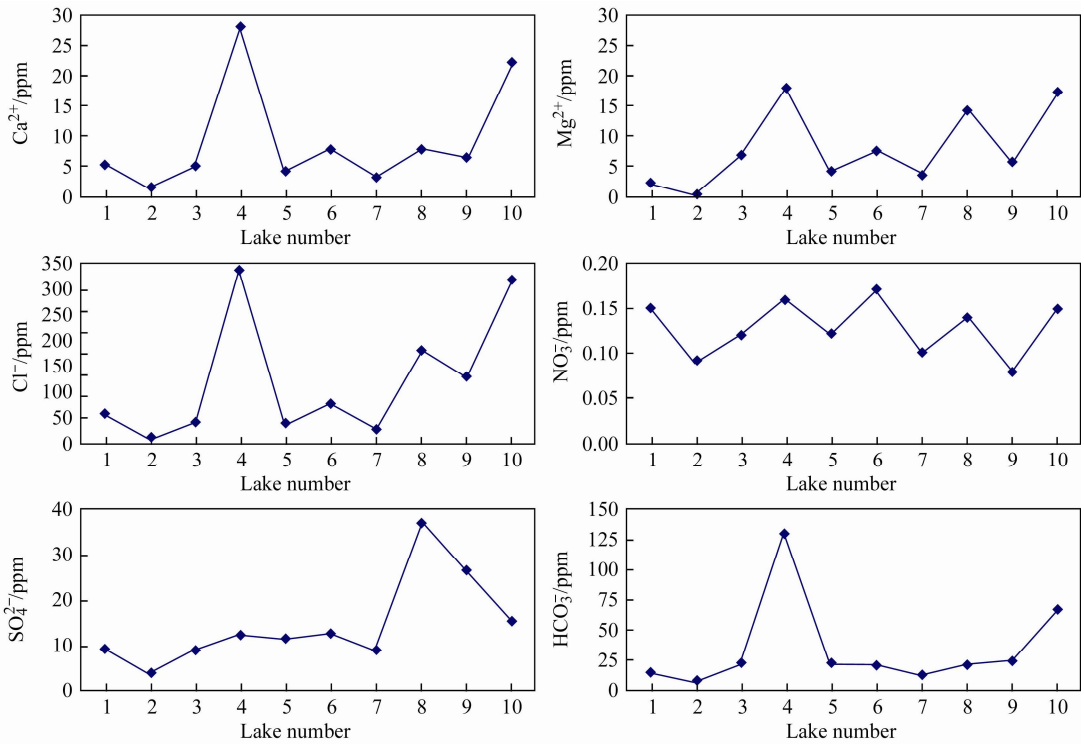

Figure 3 Physicochemical parameters and ionic concentrations of lake water samples from Fisher Island.

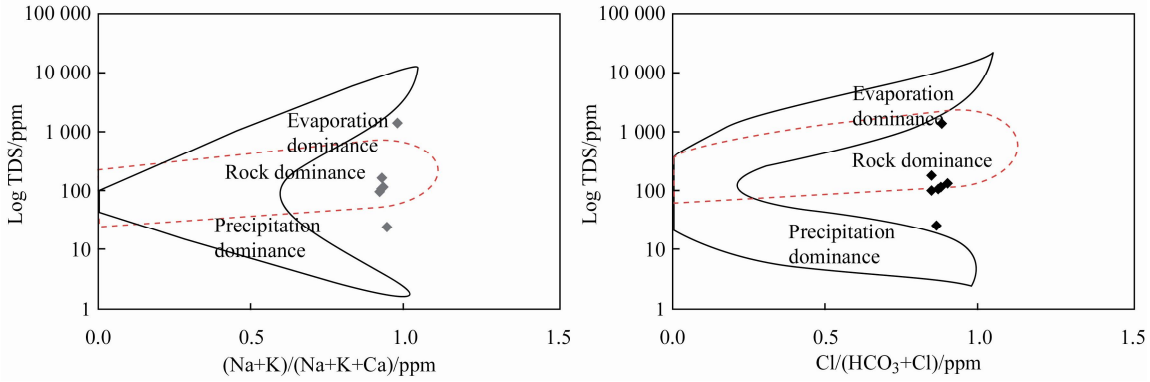

Figure 4 Plots of the major ions within the Gibb's boomerang envelope for lake water samples from Fisher Island.

Table 5 Physicochemical Characteristics and ionic concentration of lake waters from Broknes Peninsula, Larsemann Hills

Sl. No.	Sample no.	pH	EC/ (mmho·cm^{-1})	TDS	Na^+	K^+	Ca^{2+}	Mg^{2+}	Cl^-	NO_3^-	SO_4^{2-}	HCO_3^-	CO_3^-	F^-	SiO_2	B	PO_4^{3-}
1	LHE/29/BP/1B	4.63	246.3	143	51	2.3	4.8	1.5	65.3	0.23	25	12.2	0	<0.01	0.78	<0.01	0.02
2	LHE/29/BP/2B	6.94	1 040	603	177	6	14.4	22.4	309.1	0.15	45.3	48.8	0	0.05	2.02	<0.01	0.03
3	LHE/29/BP/3B	5.74	499.4	290	88	3.1	7.2	9.2	141	0.18	36.7	18.3	0	0.04	0.25	<0.01	0.02
4	LHE/29/BP/4B	6.3	437.9	254	79.7	3.8	2.4	8.3	123.1	0.18	28.6	18.3	0	0.03	0.37	<0.01	0.02
5	LHE/29/BP/5B	5.95	272.2	158	45.1	2	4	7.3	77.9	0.18	19.4	15.3	0	0.06	0.11	<0.01	0.02
6	LHE/29/BP/6B	6.23	249.1	144	35	1.8	2.4	7.8	72.9	0.24	14.8	12.2	0	0.09	<0.1	<0.01	0.02
7	LHE/29/BP/7B	6.44	348.4	202	50	2.4	4	8.8	100.5	0.1	20	15.3	0	0.05	<0.1	<0.01	0.01
8	LHE/29/BP/8B	5.91	274.5	159	43.5	1.8	4	4.9	77.9	0.13	15.7	15.3	0	0.05	<0.1	<0.01	0.03
9	LHE/29/BP/9B	6.56	381.2	221	56.3	2.6	4	9.7	108	0.14	26.7	12.2	0	0.06	<0.1	<0.01	0.02
10	LHE/29/BP/10B	7.15	655.5	380	109.2	5	8	10.7	183.4	0.15	45.6	15.3	0	0.08	0.1	<0.01	0.03

Table 6 Correlation matrix of ionic concentration of lake waters from Broknes Peninsula, Larsemann Hills

	Na^+	K^+	Ca^{2+}	Mg^{2+}	Cl^-	NO_3^-	SO_4^{2-}	HCO_3^-	F^-	SiO_2	PO_4^{3-}
Na^+	1										
K^+	0.96	1									
Ca^{2+}	0.93	0.82	1								
Mg^{2+}	0.87	0.80	0.82	1							
Cl^-	0.98	0.94	0.93	0.93	1						
NO_3^-	-0.21	-0.22	-0.22	-0.33	-0.28	1					
SO_4^{2-}	0.89	0.92	0.81	0.67	0.85	-0.15	1				
HCO_3^-	0.88	0.76	0.87	0.89	0.90	-0.20	0.59	1			
F^-	-0.03	0.02	-0.01	0.27	0.08	-0.07	0.03	-0.08	1		
SiO_2	0.79	0.67	0.80	0.69	0.77	0.05	0.53	0.91	-0.32	1	
PO_4^{3-}	0.54	0.51	0.55	0.36	0.51	-0.02	0.48	0.44	0.20	0.38	1

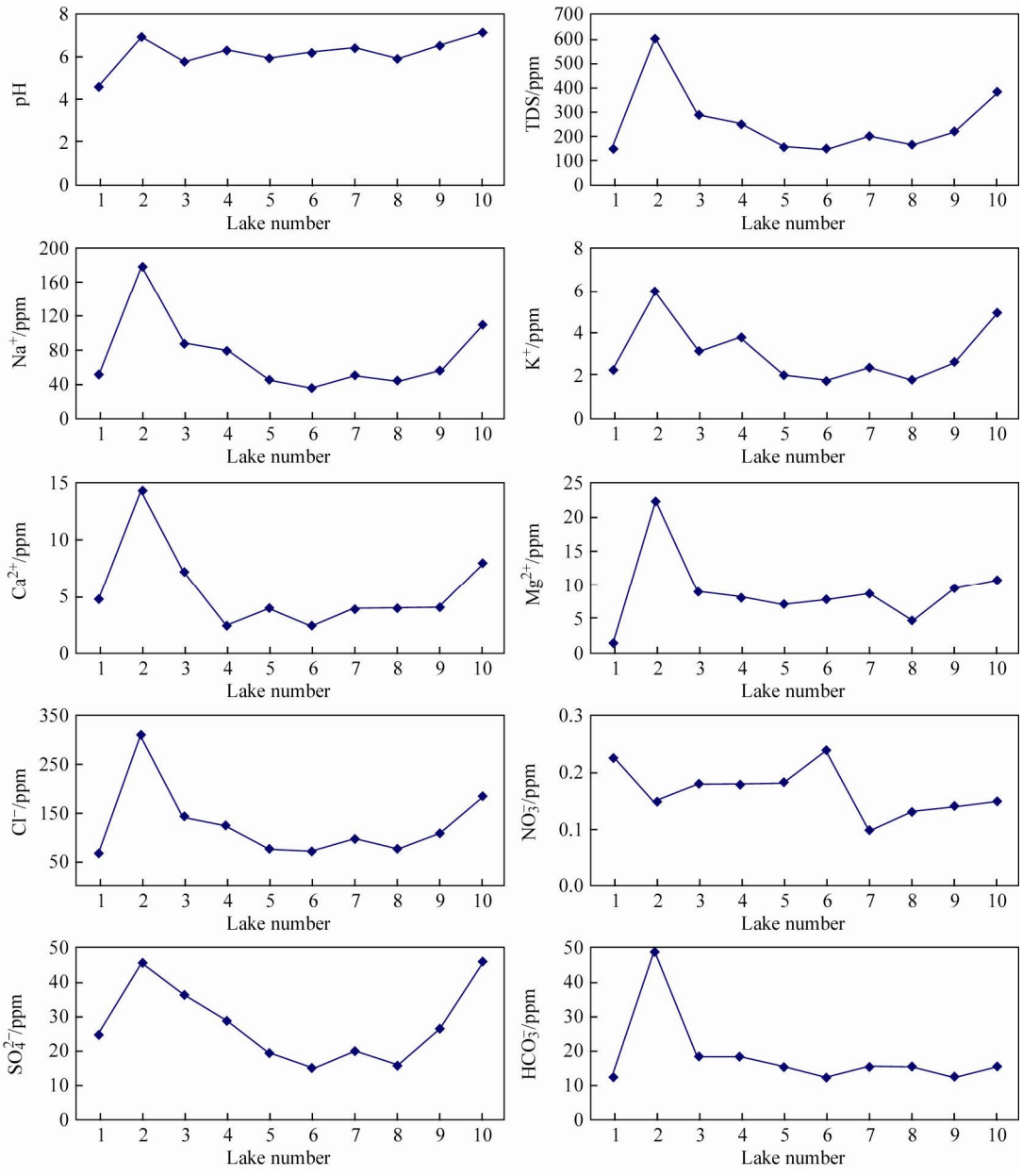

Figure 5 Physicochemical parameters and ionic concentrations of lake water samples from Broknes Peninsula.

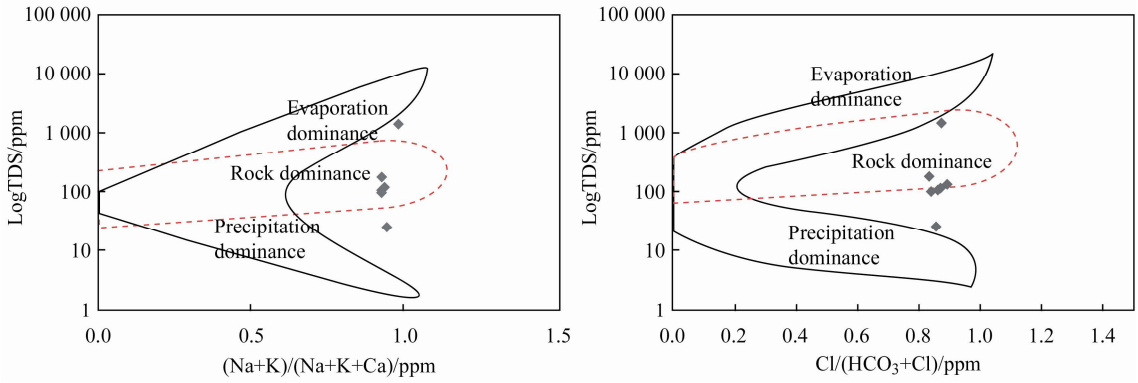

Figure 6 Plots of the major ions within the Gibb's boomerang envelope for lake water samples from Broknes Peninsula.

Major oxides, trace elements, and REE identified in the sediments of Fisher Island are listed in Tables 7 and 8. Major element plots suggest a lithic arenite to arkosic composition of the sediments (Figure 7). REE patterns of sediment samples from Fisher Island shows negative europium (Eu) anomaly (Figure 8). Results of the mechanical sieve analysis and measurements of clasts bigger than coarse sand are presented in Table 9 and frequency distribution and cumulative frequency distribution curves are shown in Figures 9 and 10, respectively. Cumulative curves are an important tool for interpreting transport mechanisms[18-21], where the three fundamental modes of sediment transport (rolling, saltation, and suspension), are identified by prominent breaks or truncations in the curves. The curves in the present study had a moderate to steep slope of 45°–70° starting from gravel to very fine silt. The statistical size parameters[18] are given in Table 10. The mean size of the sediments ranged from 0.66 to 1.81 phi, that is from coarse sand to gravel, but the standard deviation ranged from 0.81 to 2.29 indicating poor to very poor sorting of the sediments. The majority of the sediments were positively skewed but some were nearly symmetrical or negatively skewed. Negative skewness reflects the production of finer sediments by abrasion of particles from larger clasts[22]. Kurtosis, a measure of peakedness which is a function of internal sorting or distribution[23], ranged from 0.64 to 1.90 signifying a very platykurtic to a very leptokurtic structure. The spatial distribution of these parameters did not show any specific pattern in the present study area.

Table 7 Major oxides (wt.%) in sediments from Fisher Island, Larsemann Hills

S1.No.	Sample no.	SiO_2	Al_2O_3	Fe_2O_3	CaO	MgO	Na_2O	K_2O	MnO	TiO_2	P_2O_5	LOI
1	29/FI/ 1S	71.64	12.57	4.34	1.68	0.73	2.32	4.03	0.05	0.55	0.23	1.16
2	29/FI/ 1AS	72.84	11.74	2.61	1.38	0.53	2.51	4.24	0.02	0.38	0.14	1.88
3	29/FI/ 2S	71.12	13.68	2.82	1.75	0.55	3.03	4.09	0.01	0.38	0.12	0.78
4	29/FI/ 2AS	70.12	14.51	2.83	1.81	0.48	3.21	4.28	0.01	0.34	0.10	1.56
5	29/FI/ 3S	72.92	12.25	3.54	1.20	0.61	2.19	4.09	0.04	0.37	0.10	1.06
6	29/FI/ 4S	69.32	12.01	4.17	2.64	0.93	2.15	3.51	0.04	0.56	0.12	3.16
7	29/FI/ 5S	71.54	11.93	4.73	1.46	1.82	2.14	3.37	0.03	0.65	0.11	1.03
8	29/FI/ 5AS	71.98	13.14	3.51	1.77	1.41	2.74	3.19	0.02	0.46	0.09	1.04
9	29/FI/ 6S	71.31	13.35	2.84	1.65	0.69	2.80	4.47	0.01	0.40	0.14	2.58
10	29/FI/ 6AS	70.22	12.86	4.27	1.77	1.05	2.49	3.92	0.03	0.47	0.10	1.07
11	29/FI/ 7S	72.66	12.59	2.69	1.46	0.73	2.74	3.94	0.03	0.38	0.11	1.58
12	29/FI/ 7AS	70.58	12.58	3.29	1.41	0.81	2.57	3.95	0.04	0.46	0.11	4.35
13	29/FI/ 8S	68.60	13.86	5.54	1.19	0.88	2.21	3.90	0.09	0.77	0.08	1.18
14	29/FI/ 8AS	70.87	13.62	3.81	1.05	0.68	2.32	4.60	0.05	0.54	0.09	1.08
15	29/FI/ 9S	72.02	14.11	2.29	1.73	0.52	3.28	4.20	0.02	0.31	0.09	1.05
16	29/FI/ 9AS	71.90	14.02	2.34	1.72	0.52	3.24	4.15	0.02	0.31	0.09	0.94
17	29/FI/ 10S	69.18	13.90	5.46	1.20	0.89	2.16	3.94	0.09	0.76	0.08	1.09
18	29/FI/ 10AS	70.37	13.33	4.12	1.68	0.99	2.74	3.83	0.04	0.48	0.10	0.80

Table 8 Trace Element and Rare Earth Element concentrations (ppm) in lake sediments from Fisher Island, Larsemann Hills

Sample no.	29/FI/ 1S	29/FI/ 1AS	29/FI/ 2S	29/FI/ 2AS	29/FI/ 3S	29/FI/ 4S	29/FI/ 5S	29/FI/ 5AS	29/FI/ 6S	29/FI/ 6AS	29/FI/ 7S	29/FI/ 7AS	29/FI/ 8S	29/FI/ 8ASS	29/FI/ 9S	29/FI/ 9AS	29/FI/ 10S	29/FI/ 10AS
Ba	548	486	460	486	507	531	451	418	454	474	492	539	592	649	489	491	582	435
Cr	38	26	32	26	22	42	90	61	46	67	33	36	63	42	28	28	68	69
Sr	75	80	109	113	84	147	82	106	115	114	104	100	93	104	118	119	94	104
Zr	169	124	126	136	174	265	150	114	163	158	109	123	246	197	114	111	237	129
Be	1.09	0.96	1.15	1.48	1.06	0.96	1.22	1.37	1.29	1.15	1.00	1.03	0.79	0.84	1.06	0.92	0.88	1.05
Ge	1.56	1.06	1.02	1.44	1.63	1.72	1.80	1.38	1.27	1.40	1.19	1.19	1.70	1.68	1.32	1.23	2.08	1.60
Mo	1.39	1.22	1.25	1.61	1.35	1.36	1.42	1.82	0.94	0.79	0.86	1.27	1.43	1.50	0.92	1.08	1.58	0.88
In	0.05	0.02	0.03	0.05	0.05	0.07	0.09	0.06	0.05	0.07	0.04	0.05	0.07	0.04	0.03	0.03	0.07	0.07
Sn	2.70	3.36	6.09	6.11	3.44	3.61	10.53	6.98	6.88	6.69	3.15	3.18	1.66	2.58	3.90	3.44	2.02	4.64
La	72.39	43.07	60.77	70.04	63.88	95.25	107.35	80.06	44.14	74.24	58.25	67.55	84.77	59.06	43.02	42.43	90.32	74.56
Ce	102.22	76.52	85.05	109.67	104.00	144.56	157.88	114.52	82.11	98.23	87.16	91.84	115.54	118.05	94.19	86.39	157.64	127.28
Pr	12.77	9.56	10.80	11.53	11.08	15.84	17.19	12.63	9.25	11.45	10.15	10.97	14.16	10.36	8.43	8.28	14.73	11.99
Nd	46.90	33.51	36.51	43.19	41.65	59.59	63.68	44.78	33.12	39.69	34.07	36.47	47.64	39.70	31.37	30.27	54.92	43.35
Sm	10.99	7.89	8.71	8.78	8.54	11.93	13.22	9.37	7.43	8.75	7.692	8.18	10.84	7.48	6.14	5.95	10.94	8.99
Eu	1.42	1.16	1.24	1.16	1.13	1.42	1.59	1.30	1.03	1.19	1.11	1.14	1.31	1.11	0.99	0.96	1.37	1.20
Gd	10.01	6.77	7.46	7.73	7.24	9.42	10.97	7.30	6.44	6.83	5.85	6.25	8.45	6.13	5.07	4.87	9.15	7.82
Tb	1.84	1.17	1.30	1.34	1.28	1.56	1.93	1.24	1.17	1.18	1.00	1.08	1.51	1.06	0.88	0.85	1.65	1.44
Dy	9.45	5.14	5.74	6.25	6.27	7.03	9.62	5.67	5.81	5.67	4.70	5.38	8.27	5.55	4.34	4.24	9.16	7.89
Ho	1.55	0.76	0.78	0.95	0.99	1.14	1.54	0.86	0.92	0.91	0.77	0.92	1.55	0.99	0.72	0.71	1.67	1.34
Er	4.52	2.12	2.02	2.60	2.78	3.34	4.46	2.40	2.60	2.60	2.23	2.71	4.79	3.09	2.13	2.12	5.28	4.03
Tm	0.69	0.31	0.27	0.35	0.40	0.50	0.64	0.34	0.36	0.38	0.34	0.42	0.79	0.50	0.32	0.32	0.85	0.62
Yb	4.04	1.66	1.34	1.86	2.34	2.90	3.65	1.85	1.95	2.18	2.01	2.52	5.09	3.08	1.88	1.89	5.45	3.57
Lu	0.58	0.27	0.22	0.28	0.36	0.46	0.49	0.26	0.30	0.32	0.29	0.35	0.73	0.46	0.28	0.28	0.77	0.49
Hf	5.14	3.98	4.37	4.75	5.99	8.22	4.81	3.36	4.77	4.33	3.02	3.37	6.80	5.58	3.43	3.33	7.52	4.30
Ta	74.73	108.94	71.21	74.57	113.62	83.11	77.22	109.77	97	81.04	89.34	121.2	153.46	100.44	104.67	100.76	145.81	70.82
W	1 171	1 657	1 057	1 261	1 904	1 363	1 269	1 791	1 554	1 268	1 387	1 869	2 329	1 625	1 678	1 605	2 323	1 107
TI	0.20	0.23	0.22	0.15	0.17	0.14	0.11	0.10	0.16	0.15	0.16	0.17	0.15	0.12	0.14	0.14	0.12	0.24
Th	36.52	27.29	32.94	40.99	33.06	42.78	35.05	21.77	27.95	24.28	19.07	20.06	33.13	24.65	17.86	18.02	34.92	28.70
U	2.44	1.58	1.83	2.58	1.95	2.53	3.63	2.45	1.86	1.77	1.68	1.79	2.20	1.67	1.17	1.15	2.26	1.88

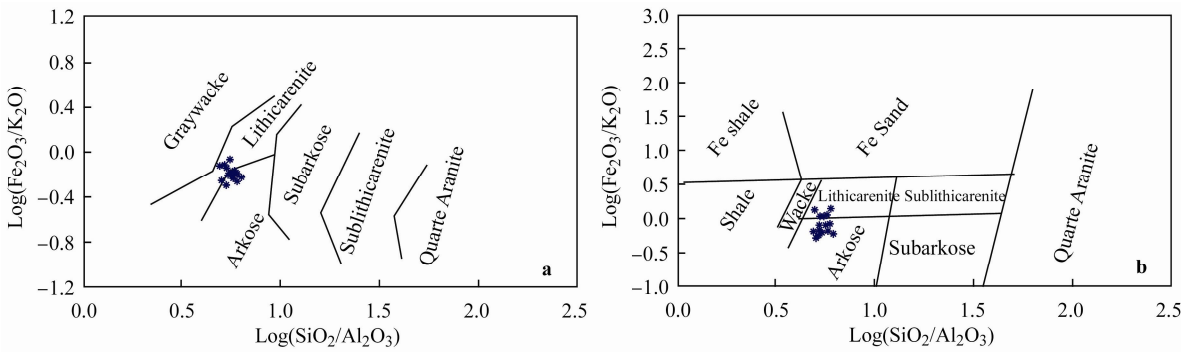

Figure 7 **a**, Composition of sediment samples from Fisher Island showing a lithic arenite composition[20]. **b**, Composition of sediment samples from Fisher Island showing an arkosic to lithic arenite composition[21].

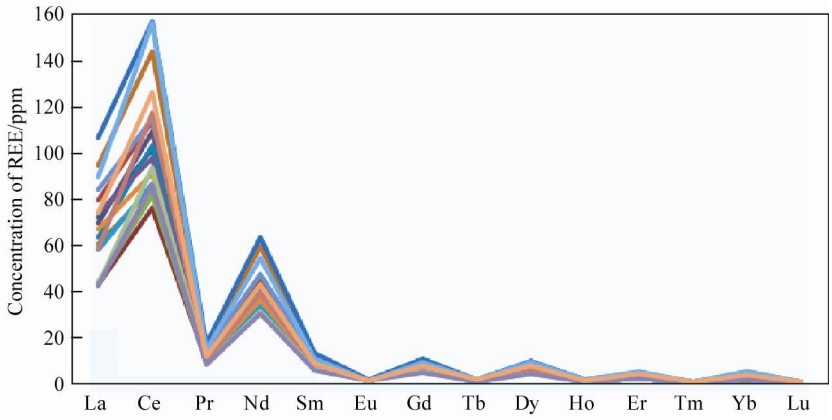

Figure 8 Frequency distribution curves of sediment samples from Fisher Island.

Table 9 Grain size analysis results of sediment samples from Fisher Island

Sl. No.	Sample no.	Physical measurement of coarse fractions					Mechanical sieve analysis											
		64 mm	32 mm	16 mm	8 mm	4 mm	+10 Mesh	10−14 Mesh	14−18 Mesh	18−25 Mesh	25−35 Mesh	35−45 Mesh	45−60 Mesh	60−80 Mesh	80−120 Mesh	120−170 Mesh	170−230 Mesh	−230 Mesh
	Φ value	-6	-5	-4	-3	-2	-1.5	-1	-0.5	0	0.5	1	1.5	2	2.5	3	3.5	4
1	29/FI/1S	0.00	0.00	6.69	10.79	8.06	25.52	7.00	8.35	3.37	11.29	8.02	4.18	4.94	1.32	0.32	0.15	0.01
2	29/FI/1AS	0.00	0.00	2.36	9.05	13.45	24.92	9.58	11.19	3.09	10.00	7.81	3.19	3.39	1.26	0.42	0.23	0.07
3	29/FI/2S	0.00	0.00	0.84	9.43	8.66	25.95	7.84	9.46	3.41	11.95	10.91	4.74	4.80	1.27	0.49	0.17	0.09
4	29/FI/2AS	0.00	0.00	4.03	9.15	6.51	19.75	8.14	9.93	3.48	13.84	11.41	5.11	5.69	1.81	0.74	0.23	0.18
5	29/FI/3S	0.00	0.00	1.08	3.66	11.21	15.91	16.88	17.53	3.94	9.81	5.20	2.18	3.19	2.02	1.30	2.70	3.38
6	29/FI/4S	0.00	0.00	0.00	4.49	7.42	11.83	7.76	7.88	2.33	9.43	5.81	4.10	7.06	4.84	3.90	11.79	11.36
7	29/FI/5S	0.00	1.57	8.48	13.94	10.64	34.48	9.90	8.53	1.81	6.15	2.92	0.82	0.43	0.11	0.09	0.13	0.01
8	29/FI/5AS	0.00	4.35	2.57	4.64	12.98	24.37	17.16	12.44	2.72	7.80	4.56	2.04	2.59	1.06	0.44	0.22	0.05
9	29/FI/6S	0.00	0.00	3.50	16.77	14.11	34.40	8.54	6.87	2.01	5.81	3.30	1.33	1.47	0.67	0.51	0.54	0.17
10	29/FI/6AS	0.00	0.00	5.94	14.33	11.11	31.34	11.31	7.82	1.73	4.56	3.07	1.48	2.27	1.41	1.06	1.20	1.37
11	29/FI/7S	0.00	0.00	0.00	1.98	3.27	5.10	7.40	15.45	4.72	24.58	17.37	7.71	8.41	2.65	0.93	0.26	0.16
12	29/FI/7AS	0.00	0.00	0.00	0.52	0.12	0.47	1.38	5.68	2.39	31.43	27.55	11.66	12.87	3.75	1.25	0.55	0.38
13	29/FI/8S	0.00	0.00	0.96	8.25	8.91	18.13	8.53	8.26	2.26	8.06	8.78	5.61	9.95	5.96	3.36	2.23	0.76
14	29/FI/8AS	0.00	0.00	2.51	8.15	11.33	22.04	7.83	6.04	1.43	5.55	6.12	4.52	9.03	6.51	4.70	2.93	1.32
15	29/FI/9S	4.15	6.72	3.96	9.58	5.26	40.06	4.40	5.10	1.27	5.95	4.89	2.49	3.58	1.50	0.66	0.31	0.13
16	29/FI/9AS	0.00	0.00	0.86	2.22	15.20	18.32	19.33	14.80	3.28	9.44	6.17	2.89	3.60	1.74	1.02	0.72	0.41
17	29/FI/10S	0.00	0.00	4.25	8.73	9.99	23.27	8.26	11.65	3.89	13.76	9.12	2.77	2.75	0.77	0.35	0.24	0.19
18	29/FI/10AS	0.00	0.00	5.78	9.13	9.00	23.90	8.57	9.76	3.75	10.53	8.26	3.67	4.43	1.61	0.82	0.46	0.33

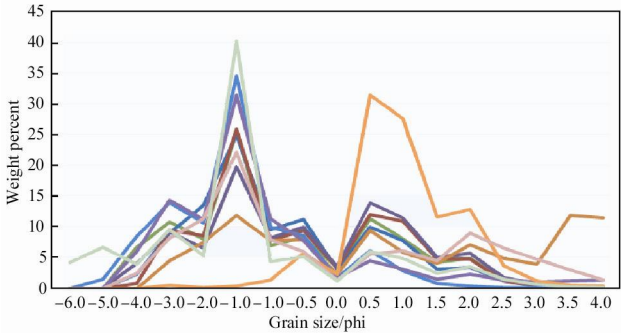

Figure 9 REE patterns of sediment samples from Fisher Island showing a negative europium (Eu) anomaly.

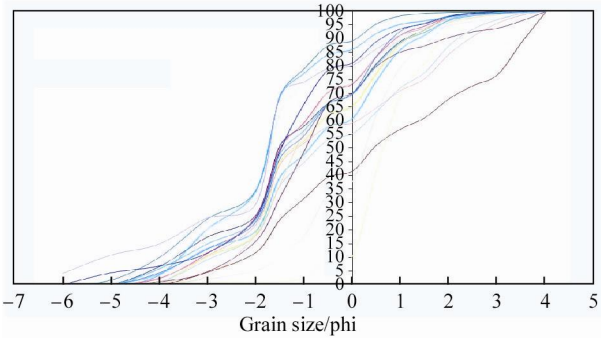

Figure 10 Cumulative frequency curves of grain size distribution in highly immature sediments from Fisher Island.

Table 10 Statistical parameters of grain size analysis of sediments from Fisher Island[28]

Sl. No.	Sample No.	Mean size (Mz)	Standard deviation (SD)	Skeweness (Sk)	Kurtosis (KG)
1	29/FI/1S	-1.35	1.85	0.12	0.98
2	29/FI/1AS	-1.18	1.59	0.23	1.03
3	29/FI/2S	-0.92	1.51	0.27	0.91
4	29/FI/2AS	-0.86	1.73	-0.01	1.00
5	29/FI/3S	-0.78	1.72	0.26	1.28
6	29/FI/4S	0.66	2.29	0.06	0.64
7	29/FI/5S	-1.55	1.84	0.01	1.29
8	29/FI/5AS	-1.30	1.65	0.06	1.90
9	29/FI/6S	-1.81	1.46	0.02	1.43
10	29/FI/6AS	-1.63	1.77	0.13	1.61
11	29/FI/7S	0.11	1.20	-0.17	1.01
12	29/FI/7AS	0.76	0.81	0.12	1.22
13	29/FI/8S	-0.34	1.95	0.17	0.84
14	29/FI/8AS	-0.57	2.11	0.33	0.80
15	29/FI/9S	-1.75	2.23	-0.07	1.55
16	29/FI/9AS	-0.92	1.40	0.28	1.05
17	29/FI/10S	-1.19	1.60	0.08	1.01
18	29/FI/10AS	-1.21	1.81	0.12	1.09

The examination of detrital quartz grains under the SEM revealed surface textures carved by the processes that operated on them during transportation and deposition. A number of researchers[16,24-28] have used SEMs to study grain morphology and surface microtextures as indicators of the sedimentary environment, transport mechanisms, and the degree of glacial crushing. Grain morphology and surface textures were examined under different magnifications and the features were grouped on the basis of individual surface textures and combinations of microtextures diagnostic of specific sediment transport mechanisms and environments. The observations are summarized in Table 11.

Table 11 Surface microtextures of quartz grains from sediment samples of Fisher Island

S1. No.	Quartz grain surface texture	Samples from lake beds	Samples from catchment area	Remarks
1	High relief	Common	Abundand	Glacial
2	Angular to subangular outline	Common	Common	Glacial
3	Subrounded to rounded outline	Common	Present	Composite (Aeolian, Glacial abrasion & aqueous transport)
4	Large conchoidal fractures	Common	Abundant	Glacial
5	Small conchoidal fractures	Present	Present	Aeolian
6	Arcuate fracture patterns/steps	Sparse	Sparse	Glacial
7	Subparallel and parallel steps	Sparse	Sparse	Glacial
8	Parallel striations	Rare	Sparse	Glacial
9	Large breakage blocks	Sparse	Sparse	Glacial grinding/crushing
10	Freshly broken smooth surfaces	Present	Common	Glacial grinding/crushing
11	Oriented scratches and grooves	Rare	Sparse	Glacial
12	Random scratches and grooves	Absent	Rare	Aeolian
13	Upturned plates	Sparse	Absent	Aeolian
14	Meandering ridges	Rare	Rare	Aeolian
15	Dish shaped concavities	Sparse	Sparse	Aeolian
16	Collision pits	Sparse	Sparse	Aeolian
17	Edge rounding/abrasion	Present	Sparse	Aeolian/Glacial

(To be continued on the next page)

(Continued)

18	Adhering particles	Sparse	Present	Glacial+Aqueous
19	Silica precipitation	Present	Rare	Aqueous/Chemical environment
20	Dissolution pits and hollows	Sparse	Rare	Aqueous/Chemical environment
21	Secondary overgrowth	Sparse	Rare	Aqueous/Chemical environment
22	Etched surfaces	Rare	Absent	Aqueous/Chemical environment

Note: Quantitative nature of occurrence classified as Abundant—> 75% observed grains exhibiting the described microtextures; Common—between 75% and 50%; Present—between 50% and 25% ; Sparse—between 25% and 10 %; Rare—<10%; Absent—0%.

Assemblages of microtextures reflecting multiple episodes of glacial crushing, aeolian transport, and varying degrees of dissolution were readily discernible. Twenty-two grain shapes and surface features were identified under the SEM (Figure 11). The oldest discernible mechanical features seen on most of the quartz grains were of glacial origin. Freshly broken and glacially abraded first generation grains that have undergone negligible aeolian or chemical actions exhibit high angularity and sharp edges. The surfaces of these grains are generally covered with mechanically produced topographical irregularities. Adhered particles or small broken parts from the body of the grain may also be identified. These surface textures were consistently observed in all samples in the present study.

4 Discussion

Four water samples from Fisher Island (Sl. No. 4, 6, 9, and 10; Table 3) were more alkaline than the other water samples. These four samples also had higher EC and TDS, mainly as a result of high levels of Na^+ (43.30–195 ppm) and Cl^- (75.40–334 ppm). However, in water sample No. 8 high levels of Na^+ (93 ppm) and Cl^- (178.40 ppm) did not correspond to a higher alkalinity. The increased alkalinity in four water samples could be a consequence of the addition of sea salt to the lake, either directly or through precipitating snow. The location of the lake could also play an important role in determining water chemistry. Smaller landlocked lakes that receive less snow melt and are poorly drained tended to have higher TDS and alkalinity.

The contribution of sea salt was supported by intra-elemental correlations (Table 4). All the major cations (Na^+, K^+, Ca^{2+}, Mg^{2+}) present in sea salt were strongly correlated with each other: $r = 0.99$, 0.95, and 0.91 for Na^+ and K^+, Na^+ and Ca^{2+}, and Na^+ and Mg^{2+}, respectively. Strong correlations between Cl^- and Na^+ ($r = 0.99$), K^+ ($r = 0.97$), Ca^{2+} ($r = 0.95$), and Mg^{2+} ($r = 0.94$) also supported the contribution of sea salt, as did the relationship between HCO_3^- and Ca^{2+} ($r = 0.96$).

In contrast to the samples from Fisher Island, the water samples from lakes on Broknes Peninsula were predominantly acidic (Table 5). The samples also differed in having less variable TDS (144–380 ppm with one peak at 603 ppm). The intra-elemental correlations were strong between Na^+ and K^+ ($r = 0.96$) and Na^+ and Ca^{2+} ($r = 0.92$), but less strong between Na+ and Mg^{2+} ($r = 0.87$). The correlations between the anion Cl^- and major cations were strong in these samples ($r > 0.9$; Table 6), however the relationship between HCO_3^- and Ca^{2+} ($r = 0.87$) was not as strong as in the samples from lakes on Fisher Island. Although the analytical data supported the contribution of sea salt to the water chemistry of lakes on Broknes Peninsula through the addition of chlorides, bicarbonates, and sulfates of cations, it also highlighted the fact that the chemistry of the water is influenced by the location of the water body. Surprisingly, samples from Lake 1 were acidic (pH 4.63) with lower TDS despite relatively high levels of recharge resulting from heavy snow accumulation in the catchment area and melting in the summer months. Further work on other lakes showing similar characteristics is needed to better explain such anomalies.

Plots of the predominant elements in sediment samples from Fisher Island suggest a lithic arenite to arkosic composition. High barium (Ba; 418–649 ppm) and strontium (Sr; 75–119 ppm) can be attributed to feldspar in the source. High tungsten (W) and tantalum (Ta) levels were most likely a result of contamination from the ball mill. High levels of zirconium (Zr; 111–265 ppm) may indicate the presence of zircon in the provenance, along with monazite as indicated by high levels of thorium (Th; 18.02–36.52 ppm) and uranium (U; 1.15–3.63 ppm). The REE enrichment (Figure 8) and well fractionated heavy rare earth elements (HREE), combined with the trace element data may indicate a granite source for these sediments. The chemical alteration index (CIA) varied between 59.08 and 65.5 indicating slight- to moderately-weathered source rock. The triangular plot between aluminum oxide (Al_2O_3), calcium oxide (CaO)+sodium oxide (Na_2O), and potassium oxide (K_2O) supported this finding[29-30]. There were no clear correlations among major oxides. However silicon dioxide (SiO_2) showed a degree of negative correlation with ferric oxide (Fe_2O_3), manganese(II) oxide (MnO), and titanium dioxide (TiO_2). Moderate negative correlations were observed between Fe_2O_3 and Na_2O, magnesium oxide (MgO) and K_2O, Na_2O and MnO, and Na_2O and TiO_2, and a degree of positive correlation was observed between Al_2O_3 and

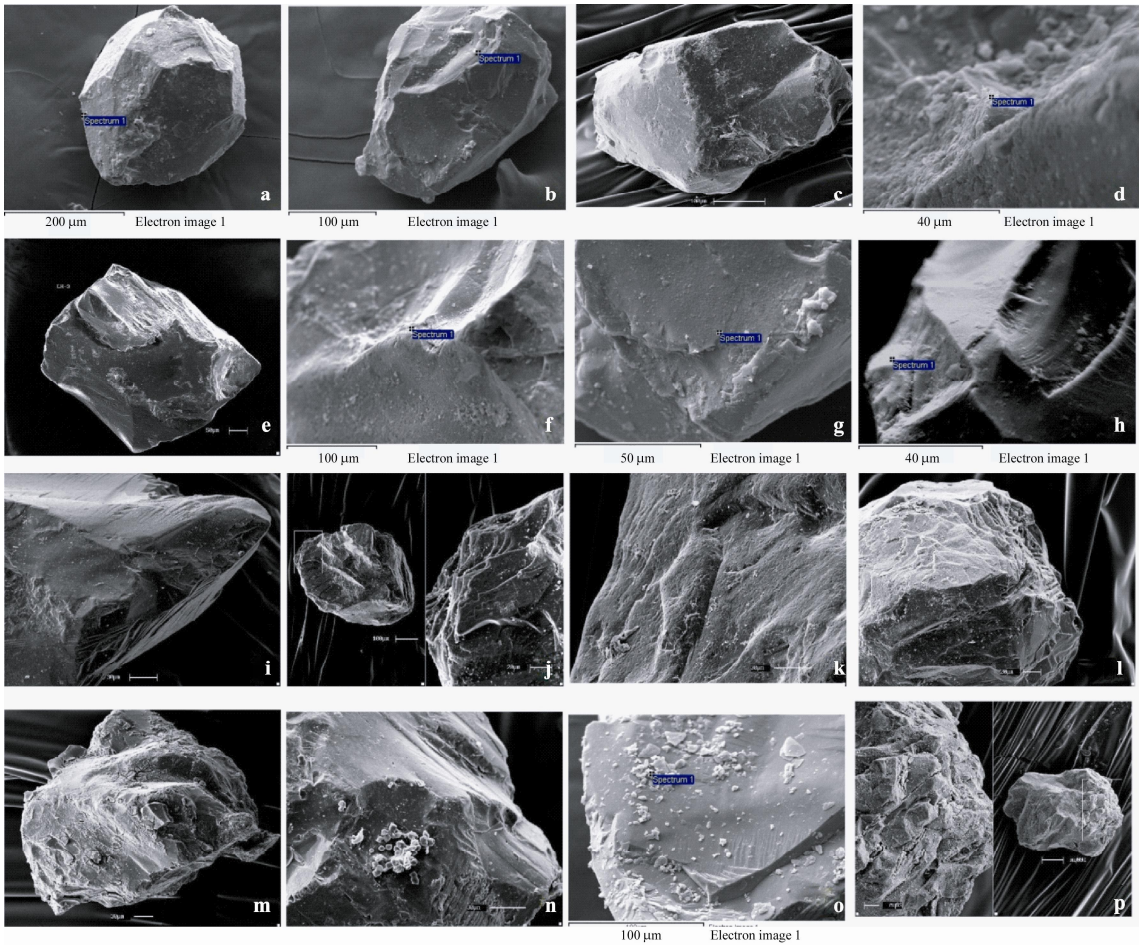

Figure 11 SEM micrographs showing composite surface features of glacial, aeolian and chemical origin. **a**, Subrounded grain showing pronounced edge rounding, remnant features of mechanical origin and minor chemical precipitation. **b**, Subrounded grain showing large, deep groove, collision pits and negligible chemical precipitation. **c**, Subangular to subrounded grain exhibiting abrasion and rounding of the edges, polished surfaces, scratches, indentations and small dish-shaped concavities, grain largely free from chemical precipitation. **d**, Magnified view of the glacial groove showing precipitation. **e**, An equant grain showing sharp edges and breakage blocks. **f**, Mechanically produced deep, circular as well as elongated grooves showing some degree of edge rounding and chemical precipitation. **g**, Irregularly broken surface produced due to intense glacial grinding, very small collision pits and chemical precipitation. **h**, Sub-surface exposures due to intense glacial grinding, sharp edges. **i**, Initially an angular, glacial grain exhibiting considerable degree of rounding, few collision pits and oriented, parallel scratches. **j**, Grain showing sub-rounded outline but conchoidal fracture patterns is still preserved. **k**, Enlarged part of a sub-rounded grain with numerous, irregularly oriented scratches, grain largely free from chemical precipitation. **l**, Part of a sub-rounded grain showing sub-parallel steps. **m**, Severely obliterated grain and the surface completely covered with chemical precipitation. Mechanically broken part of the grain bearing precipitation (**n**) and growth of euhedral crystals indicating strong chemical precipitation and immobility of the grains (**o**). **p**, Subrounded grain showing intense leaching accelerated along the fractures and irregularities of the grain.

Na_2O and Fe_2O_3 and MgO. Moderate positive correlations between Fe_2O_3 and MnO, MnO and TiO_2, and Fe_2O_3 and TiO_2 showed a strong positive correlation. Plots of the major oxides indicated a lithic arenite composition of the sediments[31-32].

There was no clear difference in the size frequency distribution among the samples because there was a wide range of scales (−5 to 3.5 phi) with a polymodal distribution. The two predominant grain size scales were −2 to −1 phi (gravel to very coarse sand) and 0 to 1.5 phi (coarse to medium sand). A characteristic feature of cumulative curves for these types of sediment is the lack of suspension with rolling and saltation because the modes of sediment transport are exposed to very high energy conditions. As supported by our findings, up to 30% of gravel and coarse sand is transported by rolling and remaining fractions are transported by saltation. Based on the distribution pattern and standard deviation of the grain size, we determined that the sediments were subjected to fluctuating energy conditions in transporting media, and reworking before final deposition. Variations in skewness and kurtosis values also suggested fluctuating energy regimes for these sediments under

different environmental conditions[24,33-34].

The microtextures and microtopographical information (Figure 11) observed on the quartz grain surfaces were predominantly intense mechanical textures characteristic of glacial transport. In most cases, several stages of crushing, grinding, and mechanical weathering were evident. The grains are mostly angular to subangular with high relief, large conchoidal fractures, deep troughs, arcuate fracture patterns, subparallel and parallel steps, striations, breakage blocks, adhering particles, oriented scratches, and grooves relating to a glacial origin. Sharp angular features and subparallel or linearly abraded grain surfaces are the hallmark of transport by ice and characterize sediment transportation by continental glaciers or ice with a thickness of >500 m[35]. Strong glacial action is also indicated by deep striations and polished surfaces[36-37]. Different types of mechanical microtextures including conchoidal fractures, straight and curved grooves, and troughs are formed by transport in the basal zone of continental glaciers[35,38]. Quartz grains with aeolian microtextures obliterate the first order mechanical textures produced by glacial grinding and crushing. The most common aeolian feature is pronounced edge rounding that imparts a high degree of roundness and sphericity. Pronounced edge rounding, pitted surfaces, dish shaped concavities, and other aeolian features indicate strong anabatic and katabatic polar wind action.

Features of a chemical origin, including mild dissolution etching and silica precipitation in the form of amorphous and cryptocrystalline overgrowth, suggest precipitation on immobile grains in the lacustrine environment. Features of a chemical origin are the youngest observed on quartz grains and occur in the form of minor to deep dissolution pits and etching, and chemical precipitations within the topographical irregularities. Minor dissolution effects indicate fewer interactions with aqueous media and a relatively fresher contribution of sediments to the lacustrine system. Deep dissolution cavities, cryptocrystalline precipitations, and euhedral crystal growth signify strong chemical activity after deposition and subsequent diagenetic changes and immobility of grains in the lacustrine environment.

5 Conclusions

The Larsemann Hills are part of an ice-free coastal oasis in Prydz Bay, an embayment on the East Antarctic margin. Among the islands and peninsulas in the deglaciated terrain of the Larsemann Hills, Fisher Island and Broknes Peninsula constitute two important landmasses falling within the polar lowland periglacial climatic regime characterized by low precipitation, and low rates of ice melt and sediment influx into the lacustrine system. The landlocked lakes occur in the typical physiographic setting of the proximal ice-sheet and marine ecosystems. The following conclusions are drawn from the findings of the present investigation including field observations, chemical analysis of lake water, and sedimentological studies based on grain size analysis and SEM examination of surface textures.

The pH values in lake water from Fisher Island ranged from 6.75 to 8.2, indicating slightly acidic to weakly alkaline conditions. Wide variations in EC (26–1 179 mmho·cm^{-1}) and TDS (15–684 ppm) were recorded in the water samples. Lake waters from Broknes Peninsula had pH values ranging from 4.63 to 7.15 indicating acidic to near neutral conditions with only one lake (No. 10) showing weakly alkaline conditions. The EC ranged from 246.3 to 1 040 mmho·cm^{-1} and TDS ranged from 143 to 603 ppm.

In general, the lakes on Fisher Island had lower EC and TDS than the lakes on Broknes Peninsula. This difference can be attributed to the greater freshwater input to the Fisher Island lakes, or to the longer time elapsed since deglaciation on Broknes Peninsula, which is thought to have remained exposed during the Last Glacial Maximum.

Unconsolidated deposits were sparsely distributed in the area which is dominated by bare rock slopes with a patchy and scattered covering of glacial sediments, valley fills, and occasional moraine ridges. The glacial debris are redistributed in small basins and depressions in surface run-off due to glacial melt and by strong polar winds. The paucity of sediments in the catchment areas and within the lake systems can be attributed to the combined effects of the relatively low volume and availability of sediments, transportation and deposition by ice, and paraglacial processes that redistribute and concentrate deposits during and after deglaciation.

Based on the plots of major oxides, the chemistry of sediments from Fisher Island showed a lithic arenite to arkosic composition[20-21]. The CIA for these sediments varied between 59.08 and 65.5, indicating slightly- to moderately-weathered source rocks[18-19]. The depositional process takes place during the short summer period with limited surface run-off from glacial melt that erodes and transports surface debris through small seasonal streams. Sediments on Fisher Island were immature and poorly to very poorly sorted, consisting of gravelly sand with negligible silt and finer fractions. Grain size distribution showed a polymodal character with two major populations between −2 to −1 phi (gravel to very coarse sand) and 0–1.5 phi (coarse to medium sand). Up to 30% of gravel and coarse sand are transported by rolling, and remaining fractions are transported by saltation.

Microtextures observed on the quartz grain surfaces under SEM are dominated by intense mechanical textures characteristic of glacial transport. Several stages of crushing, grinding, and mechanical weathering were noted. The quartz grains also exhibited aeolian microtextures, represented by edge rounding, which overprinted the first order mechanical textures produced by glacial grinding. Chemical features on the grains are the last to form and were represented by mild to deep dissolution etching and precipitation within the surficial irregularities. Mild dissolution may indicate a lesser interaction with aqueous media and a relatively new contribution of sediments to the lacustrine system. The presence of deep dissolution cavities, cryptocrys-

talline precipitation, and euhedral crystal growth may signify strong chemical activity after deposition and immobility of the grains in the lacustrine environment.

Acknowledgements RA wishes to express his gratitude to the Director General of GSI for nominating him to lead the voyage of the 29th Indian Antarctic Expedition (2009–2010) during which the water and sediment sampling was carried out. All authors wish to thank the National Centre for Antarctic and Ocean Research, Goa, for supporting the Indian Antarctic expeditions and the XII and XIII Asian Forum for Polar Sciences (AFoPS) sessions conducted in India.

References

1 Gillieson D S. An environmental history of two freshwater lakes in the Larsemann Hills, Antarctica. Hydrobiologia, 1991, 214(1): 327-331.
2 Priddle J R, Heywood B. Evolution of Antarctic lake ecosystems. Biol J Linn Soc, 1980, 14(1): 51-66.
3 Burgess J S, Spate A P, Shevlin J. The onset of deglaciation in the Larsemann Hills, Eastern Antarctica. Antarct Sci, 1994, 6(4): 491-495.
4 Burgess J, Carson C, Head J, et al. Larsemann Hills: Not heavily glaciated during the Last Glacial Maximum // Ricci C A. The Antarctic Region: Geological Evolution and Processes. Siena: Universtà degli Studi di Siena, 1997: 841-843.
5 Verleyen E, Hodgson D A, Sabbe K, et al. Late Quaternary deglaciation and climate history of the Larsemann Hills (East Antarctica). J Quart Sci, 2004, 19(4): 361-375.
6 Fitzsimons S J. Paraglacial redistribution of glacial sediments in the Vestfold Hills, East Antarctica. Geomorphology, 1996, 15(2): 93-108.
7 Fitzsimons S J. Depositional models for moraine formation in East Antarctic coastal oases. J Glaciol, 1997, 43(144): 256-264.
8 Hodgson D A, Verleyen E, Sabbe K, et al. Late quaternary climate driven environmental change in the Larsemann Hills, East Antarctica, Multi Proxy evidence from a lake sediment core. Quat Res, 2005, 64(1): 83-99.
9 Ellis-Evans J C, Laybourn-Parry J, Bayliss P R, et al. Physical, chemical and microbial community characteristics of lakes of the Larsemann Hills, Continental Antarctica. Arch für Hydrobiol, 1998, 141(2): 209-230.
10 10 Shrivastava P K, Asthana R, Beg M J, et al. Ionic characters of lake water of Bharti Promontory, Larsemann Hills, East Antarctica. J Geol Soc India, 2011, 78(3): 217-225.
11 Asthana R, Shrivastava P K, Beg M J, et al. Sedimentary processes in two different polar periglacial environments: Examples from Schirmacher Oasis and Larsemann Hills, East Antarctica. J Geol Soc London, 2013, 381(1): 411-427.
12 Gasparon M, Burgess J S, Sigurdsson I A, et al. Natural and anthropogenic sources of trace metals in fresh water lakes of the Larsemann Hills, East Antarctica//International workshop Larsemann Hills: an Antarctic microcosm. Hobart: AAD Int. Workshop, 1997: 13-16.
13 Krinsley D H, Doornkamp J C. Atlas of quartz sand surface textures. New York: Cambridge University Press, 1973: 91.
14 Ingolfsson O. Quaternary glacial and climatic history of Antarctica // Ehlers J, Gibbard P L. Quaternary Glaciations-Extent and Chronology, Pt. III: South America, Asia, Africa, Australia, Antarctica. New York: Elsevier, 2004: 3-43.
15 Gibbs R J. Mechanisms controlling world water chemistry. Science, 1970, 170(3962): 1088-1090.
16 Håkansson L, Jansson M. Principles of lake sedimentology. Berlin, Heidelberg: Springer-Verlag, 1983: 316.
17 Gilbert R, Chong Å, Dunbar R B, et al. Sediment trap records of glacimarine sedimentation at Müller Ice shelf, Lallemand Fjord, Antarctic Peninsula. Arctic Antarct Alp Res, 2003, 35(1): 24-33.
18 Nesbitt H W, Young G M. Prediction of some weathering trends of plutonic and volcanic rocks based on thermodynamic and kinetic considerations. Geochim Cosmochim Ac, 1984, 48(7): 1523-1534.
19 Nesbitt H W, Young G M. Formation and diagenesis of weathering profile. J Geol, 1989, 97(2): 129-147.
20 Pettijohn F J, Potter P E, Siever R. Sand and sandstone. New York: Springer, 1972: 618.
21 Herron M M. Geochemical classification of terrigenous sands and shales from core or log data. J Sediment Petrol, 1988, 58(5): 820-829.
22 Sindowski K H. Die synoptische methode des Kornkurven-Vergleiches Zur Ausdeutung fossiler sedimentationsraume. Geol Jahrb, 1958, 73: 235-275.
23 Fuller A O. Size distribution characteristics of shallow marine sands from the cape of Good Hope, South Africa. J Sediment Petrol, 1961, 31(2): 256-261.
24 Friedman G M. Dynamic processes and statistical parameters compared for size frequency distribution of beach and river sand. J Sediment Petrol, 1967, 37: 327-354.
25 Visher G S. Grain size distributions and depositional processes. J Sediment Petrol, 1969, 39(3): 1074-1106.
26 Boulton G S. Boulder shapes and grain-size distributions of debris as indicators of transport paths through a glacier and till genesis. Sedimentology, 1978, 25(6): 773-799.
27 Cadigan R A. Geologic interpretation of grain-size distribution measurements of Colorado Plateau sedimentary rocks. J Geol, 1961, 69(2): 129-144.
28 Folk R L, Ward W C. Brajos river bar: a study in the significance of grain size parameters. J Sediment Petrol, 1957, 27(1): 3-26.
29 Mason C C, Folk R L. Differentiation of beach, dune, and aeolian flat environments by size analysis, Mustang Island, Texas. J Sedment Petrol, 1958, 28(2): 211-226.
30 Asthana R, Chaturvedi A. The grain size behaviour and morphoscopy of supraglacial sediments, South of Schirmacher Oasis, E. Antarctica. J Geol Soc Ind, 1998, 52: 557-568.
31 Krinsley D H, Donahue J. Environmental interpretation of sand grain surface textures by electron microscopy. Geol Soc Am Bull, 1968, 79(6): 743-748.
32 Margolis S V, Krinsley D H. Processes of formation and environmental occurrence of microfeatures on detrital quartz grains. Am J Sci, 1974, 274(5): 449-464.
33 Mahaney W C. Pleistocene and Holocene glacier thicknesses, transport histories and dynamics inferred from SEM microtextures on quartz particles. Boreas, 1995, 24(4): 293-304.
34 Shrivastava P K, Asthana R, Roy S K, et al. Provenance and depositional environment of epi-shelf lake sediment from Schirmacher Oasis, east Antarctica, vis-à-vis scanning electron microscopy of quartz grain, size distribution and chemical parameters. Polar Sci, 2012, 6(2): 165-182.
35 Krinsley D, Margolis S. Section of geological sciences: A study of quartz sand grain surface textures with the scanning electron microscope. Trans NY Acad Sci, 1969, 31(5 Series II): 457-477.
36 Krinsley D H, Smith D B. A selective SEM study of grains from the Permian yellow sands of north-east England. Proc Geol Assoc, 1981, 92(3): 189-196.
37 Mahaney W C, Kalm V. Scanning electron microscopy of Pleistocene tills in Estonia. Boreas, 1995, 24(1): 13-29.
38 Mahaney W C, Claridge G, Campbell I. Microtextures on quartz grains in tills from Antarctica. Palaeogeogr Palaeocl, 1996, 121(1-2): 89-103.